Draft version March 25, 2025
Typeset using LaTeX default style in AASTeX63



# Self-Organized Criticality Across Thirteen Orders of Magnitude in the Solar-Stellar Connection

Markus J. Aschwanden & Carolus, J. Schrijver[1]

[1] *Lockheed Martin, Solar and Astrophysics Laboratory (LMSAL), Advanced Technology Center (ATC), A021S, Bldg.252, 3251 Hanover St., Palo Alto, CA 94304, USA; e-mail: markus.josef.aschwanden@gmail.com*

## ABSTRACT

The observed size distributions of solar and stellar flares is found to be consistent with the predictions of the fractal-diffusive self-organized criticality (FD-SOC) model, which predicts power law slopes with universal constants of $\alpha_F = (9/5) = 1.80$ for the flux, and $\alpha_E = (5/3) \approx 1.67$ for the fluence, respectively. In this Letter we explore the solar-stellar connection under this aspect, which extends over an unprecedented dynamic range of 13 orders of magnitude between the smallest detected solar nanoflare event ($E_{min} = 10^{24}$ erg) and the largest superflare ($E_{max} = 10^{37}$ erg) on solar-like G-type stars, observed with the KEPLER mission. The FD-SOC model predicts a scaling law of $L \propto E^{(2/9)}$ for the length scale $L$ as a function of the flare energy $E$, which limits the largest flare size to $L_{max} \lesssim 0.14 R_\odot$ for solar flares, and $L_{stellar} \lesssim 1.04\ R_\odot$ for stellar flares on G-type stars. In the overall we conclude that the universality of power laws (and their slopes) is a consequence of SOC properties (fractality, classical diffusion, scale-freeness, volume-flux proportionality), rather than identical physical processes at different wavelengths.

*Keywords:* methods: statistical — fractal dimension — self-organized criticality —

## 1. INTRODUCTION

The concept of self-organized criticality (SOC) was originally proposed by Bak, Tang, & Wiesenfeld (1987) and has been used in over 6000 publications since. An interdiscipliary approach of SOC phenomena is sketched in the book by Bak (1996). The SOC paradigm can be understood most easily with the sandpile analogy. If you trickle sand grains on top of a sandpile, the slope (or angle of repose) on the inclines of the sandpile start to steepen until the system reaches a critical angle (which is about 38° in real-world sandpiles). Every additional sand grain dropped onto the critically inclined slope will trigger a small or a large avalanche, which is a highly nonlinear process. Bak et al. (1987) developed the ingenious method of using a n-dimensional lattice grid to simulate next-neighbor interactions with a computer code. The "critical" sandpile is driven by the balance between the input (infalling sand grains) and the output (or avalanches running off the boundaries at the bottom of the sandpile). If the avalanche duration is shorter than the waiting time interval between subsequent avalanches, the system is said to be slowly driven. The sandpile experiments of Bak et al. (1987) produced power law distribution functions with slopes of $\alpha_S = 1.37$ for the avalanche size $S$, and $\alpha_T = 0.92$ for avalanche durations $T$, respectively. Extensive literature on this type of numerical SOC simulations can be found in Pruessner (2012).

About two decades later, after the execution of numerous SOC simulations in discretized n-dimensional space, a paradigm shift occurred that has been named the *fractal-diffusive self-organized criticality (FD-SOC)* model (see textbooks by Aschwanden 2011, 2025). The new approach is motivated by the dilemma that microscopic real-world simulations are computationally expensive, if not impossible, such as in the case of bridging microscopic (atomic) scales to macroscopic scales (measurable in a "real-world" scenario). Moreover, next-neighbor interactions have to be simulated with iterative steps, which makes it to a mathematically infinite equation system. Instead, next-neighbor interactions can be approximated by the classical diffusion process, and the spatial inhomogeneity of SOC avalanches can be approximated by fractal dimensions. This way the power law size distributions can be quantified with simple (macroscopic) physical scaling laws, which obey the scale-freeness in their statistical probability distribution functions.

[1] This paper is dedicated to Carolus J. Schrijver (1958-2024) in memoriam.

It appears that the FD-SOC model is a suitable description for many astrophysical (solar and stellar) phenomena, but has also wide-spead applications in geophysics, biophysics, medical sciences, as well as in financial physics. More detailed descriptions of the FD-SOC model can be found in Aschwanden (2014, 2015), Aschwanden et al. (2016, 2021, 2022), Aschwanden & Gogus (2025), while alternative SOC reviews are given elsewhere (Aschwanden et al. 2013, 2016; Watkins et al. 2016; Sharma et al. 2016; McAteer et al. 2016).

The contents of this Letter includes observations (Chapter 2), data analysis (Chapter 3), discussion (Chapter 4), and conclusions (Chapter 5).

## 2. OBSERVATIONS

We use multiple data sets to synthesize a joint size distribution, selected by their published power law slopes $\alpha_E$ and energy ranges $E_{min}, E_{max}$ of their energy (in physical units [erg]), not to be confused by their power law slopes of peak fluxes $\alpha_F$, which are quantified in physical units of [erg/s]. A synthsized size distribution, as composed by 5 individual size distributions, is fitted to a theoretically predicted power law slope, as shown in Fig. (1). While the power law slopes are invariant accross 13 orders of magnitude, the energy definitions of these individual data sets are not homogeneous here. In the following, we subdivide the data sets into three groups according to the used energy definitions and wavelength dependence (Table 1): (i) thermal energies, radiating in soft X-rays (SXR), extreme-ultraviolet (EUV), and ultraviolet (UV); (ii) non-thermal energies (radiating in hard X-rays and gamma rays), and (iii) bolometric energies, radiating in white light.

### 2.1. *Soft X-Ray Thermal Energies*

The smallest solar flare events, also called “nanoflares” or “transient brightenings”, were sampled by observations with SXT/Yohkoh (Shimizu 1995), EIT/SOHO (Krucker & Benz 1998; Benz & Krucker 2002; TRACE (Aschwanden et al. 2000; Parnell & Jupp 2000), and GOES (Li et al. 2012).

The physical parameters of nanoflares include electron temperatures of $T_e \lesssim 2$ MK, electron densities of $n_e \approx\ \lesssim 10^9$ cm$^{-3}$, (loop) length scales of $L = 2 - 20$ Mm, and thermal energies of $E_{th} = 10^{24} - 10^{26}$ erg (Aschwanden et al. 2000). In comparison, the physical parameters of transient brightenings cover electron temperatures of $T_e \approx 4-8$ MK, electron densities of $n_e \approx 2 \times 10^9$ cm$^{-3}$ $- 2 \times 10^{10}$ cm$^{-3}$, (loop) length scales of $L = 5 \times 10^3$ km to $4 \times 10^4$ km, durations of $T = 2 - 7$ min, and thermal energies of $10^{26} - 10^{29}$ erg (Shimizu 1995).

Other studies yield similar values (Krucker & Benz 1998; Benz & Krucker 2002; Parnell & Jupp 2000), Li et al. 2012, in Fig.7 therein), but cannot be compared with the 3-D standard FD-SOC model here, since they use a 2-D model that results into steeper power law slopes of $\alpha_E \gtrsim 2.3 - 2.6$ for the flare energy. Generally, the thermal energy is defined by

$$E_{th} = 3 k_B T_e n_e V = 3 k_B T_e \sqrt{EM \times V \times f} \ , \qquad (1)$$

where $k_B$ is the Boltzmann constant, $EM = n_e^2 V$ is the volumetric emission measure, $V$ is the flare volume, and $f$ is a filling factor. In early studies the volume has been quantified by a flare area $A$ and a constant line-of-sight depth $h_0$, i.e., $V = A\ h_0$, which corresponds to a 2-D (flat-world) model. Moreover, the fractality of the spatial inhomogeneity is ignored with a constant line-of-depth $h_0$. Hence, a definition that is more consistent with the FD-SOC model is, after inserting of $n_e = \sqrt{EM \times V}$,

$$E_{th} = 3 k_B T_e n_e V = 3 k_B T_e \sqrt{EM \times L^{D_V}} \ , \qquad (2)$$

where $D_V$ is the fractal (Hausdorff) dimension and has a mean value of $D_V = 2.5$ in a 3-D world.

### 2.2. *Hard X-ray Nonthermal Energies*

Size distributions of solar non-thermal flare energies have been sampled from ISEE-3/ICE (Lu et al. 1993), and from HXRBS/SMM data (Crosby et al. 1993). The latter data set contains a number of $N_{\rm HXRBS} = 11,352$ flare events and has been accumulated over an observational epoch of $T_{\rm HXRBS} \approx 11$ [years] (Crosby et al. 1993; Aschwanden et al. 2017). The total energy in electrons ($>$ 25 keV) is found to cover a range of $E_{\rm HXR} \approx 3 \times 10^{28} - 10^{31}$ erg, as computed from the non-thermal electron energy radiated in hard X-ray (HXR) wavelengths at $\geq 25$ keV with the HXRBS detectors onboard the SMM spacecraft (Dennis et al. 1985), assuming the thick-target bremsstrahlung model (Brown 1971). The energy in nonthermal electrons for the thick-target model is given by (Brown 1971; Crosby et al. 1993),

$$F(> E_0) = 4.8 \times 10^{24} A E_0^{-\gamma+1} E_m^{\gamma} \gamma(\gamma - 1) \beta(\gamma - \frac{1}{2}, \frac{1}{2}) \quad [\text{erg s}^{-1}] \ , \qquad (3)$$

where $\beta$ is the beta function, and $E_0$ is the cut-off energy. The power law slopes are found to be essentially invariant during the solar cycle, with best-fit values of $\alpha_E = 1.53 \pm 0.02$, $1.51 \pm 0.04$, $1.48 \pm 0.02$, and $1.53 \pm 0.02$ during the year ranges of 1980-1982, 1983-1984, 1985-1987, and 1988-1989, which can be compared with the theoretical FD-SOC model prediction of $\alpha_E = (5/3) \approx 1.67$.

### 2.3. *White-Light Bolometric Energies*

Homogeneous searches for stellar flares in every available KEPLER light curve (Borucki et al. 2010) revealed up to 851,168 candidate flare events, which have an average flare energy of $\approx 10^{35}$ erg (Davenport 2016). A KEPLER flare catalog with a sample of 162,262 events that supposedly controls false-positive signals and artifacts of earlier data sets revealed a power law slope of $\alpha_E \approx 2$, from which a superflare with an energy of $\approx 10^{34}$ was estimated to occur on the Sun at least once in 5500 [years] (Yang & Liu 2019). For stellar flares we use the KEPLER data set of G-type stars, which is most similar to the solar flare data set, with the Sun being classified as a G5-type star. This stellar data set comprises $N_{\rm KEPLER} = 55,269$ stellar flares and is observed during a time period of $T_{\rm KEPLER} \approx 5$ [years] (Aschwanden & Güdel 2021). $E_{\rm bol}$ represents the energy of the bolometric (white-light) luminosity in the wavelength range of $\lambda \approx 4300 - 8900$ Å with the KEPLER instrument. The wavelength range of KEPLER ($4300 - 8900$ Å) overlaps with the green line ($5548 - 5552$ Å), the red line ($6682 - 6686$ Å), and the blue line ($4502 - 4506$ Å).

Following Namekata et al. (2017a), there are two differences between solar and stellar observations: time cadences and passbands. HMI/SDO observes the overall Sun with a 45 s cadene and a narrowband filtergram around an Fe $\lambda$ 6173.3 line, while KEPLER carried out 1-minute cadence observations with $4000{-}9000$ Å broadband filters. The white-light solar flare energy $E_{wl}$ is radiated by a temperature $T_{flare} = 10,000$ K, and is calculated as

$$E_{wl} = \sigma_{\rm SB} T_{flare}^4 \int A_{flare}(t) dt \ , \tag{4}$$

with the stellar flare area $A_{flare}$ defined by,

$$A_{flare}(t) = {L_{flare} \over L_{Sun}} \pi R^2 {\int R_\lambda B_\lambda(5800 \ {\rm K}) \ d\lambda \over R_\lambda B_\lambda(T_{flare}) d\lambda} \ , \tag{5}$$

where $\sigma_{\rm SB}$ is the Stefan-Boltzmann constant, $L_{flare}/L_{Sun}$ is the flare luminosity ratio to the overall luminosity, $R$ is the solar radius, $R_\lambda$ is a response function of HMI/SDO, and $G_\lambda(T)$ is the Planck function at a given wavelength $\lambda$.

## 3. THEORY OF THE FD-SOC MODEL

In the following we describe briefly a definition of the *Fractal-Diffusive Self-Organized Criticality (FD-SOC)* model, while more extensive descriptions can be found in textbooks and review papers (Aschwanden 2014, 2015, 2022, 2025; Aschwanden et al. 2016). The FD-SOC model is based on four fundamental assumptions: (i) the 3-D dimensionality, (ii) the mean fractal (Hausdorff) dimension, (iii) the scale-freeness probability distribution function, and (iv) the volume-flux proportionality for incoherent emission processes.

Instead of using the next-neighbor interactions of cellular automata, as defined in the original SOC model of Bak (1987), we quantify the spatial inhomogeneity in terms of the fractal dimension $D_d$ for the Euclidean domains $d = 1$ (lines), $d = 2$ (areas), or $d = 3$ (volumes). Each fractal domain has a maximum fractal dimension of $D_d = d$, a minimum value of $D_d = (d - 1)$, and a mean value of $D_V = d - 1/2$,

$$D_V = {(D_{\rm V,max} + D_{\rm V,min}) \over 2} = d - {1 \over 2} \ . \tag{6}$$

For most applications in the (observed) 3-D world, the dimensional domain $d = 3$ is appropriate, which implies a fractal dimension $D_V = 2.5$. However, if 2-D areas are observed, the fractal dimension is $D_A = 1.5$ and the dimensionality is $d = 2$. In this work we will mostly make use of the 3-D fractal domain, while the 2-D domain is discussed elsewhere (e.g., Aschwanden 2022). The fractal volume $V$ is then defined by the standard (Hausdorff) fractal dimension $D_V$ in 3-D and the length scale $L$ (Mandelbrot 1977),

$$V(L) \propto L^{D_V} \ . \tag{7}$$

We formulate the statistics of SOC avalanches in terms of size distributions (or occurrence frequency distributions) that obey the scale-free probability distribution function (Aschwanden 2014, 2015, 2022), expressed with the power law function

$$N(L) \ dL \propto L^{-d} dL \ , \tag{8}$$

where $d = 1, 2, 3$ represent the Euclidean dimensions of the fractal domains and $L$ is the length scale of a SOC avalanche. From this scale-free relationship, the power-law slopes $\alpha_x$ of other SOC parameters $x = [A, V, F, E, T]$ can be derived, such as for the area $A$, the volume $V$, the flux $F$, the fluence or energy $E$, and the duration $T$. The resulting power-law slopes $\alpha_x$ can then be obtained mathematically by the method of variable substitution $x(L)$, by inserting the inverse function $L(x)$ and its derivative $|dL/dx|$,

$$N(x)dx = N[L(x)] \left| \frac{dL}{dx} \right| dL = \ x^{-\alpha_x} dx \ , \tag{9}$$

such as for the flux $x = F$,

$$\alpha_F = 1 + \frac{(d-1)}{D_V \gamma} = \frac{9}{5} = 1.80 \ , \tag{10}$$

or for the fluence $x = E$,

$$\alpha_E = 1 + \frac{(d-1)}{d\gamma} = \frac{5}{3} = 1.67 \ . \tag{11}$$

$\gamma$ is the nonlinearity coefficient in the flux-volume relationship,

$$F \propto V^\gamma = \left( L^{D_V} \right)^\gamma \ , \tag{12}$$

which degenerates to proportionality $F \propto V$ for $\gamma = 1$. Note that the definitions of the peak flux $F$ and fluence $E$ differ only by the fractal dimension $D_V$ (Eq. 10) and the (space-filling) Euclidean dimension $d$ (Eq. 11). In astrophysical high-temperature plasmas, the volume $V$ is approximately proportional to the number of electrons in a region of instability, while the flux $F$ is proportional to the number of emitting photons, which implies that the photon-to-electron ratio is approximately constant and justifies the assumption of the flux-volume proportionality, in the case of incoherent emission mechanisms.

While this brief derivation of Eqs. (5-11) expresses the main assumptions of fractality and linear flux-volume relationship for $\gamma = 1$, an additional assumption needs to be brought in that takes the spatio-temporal evolution into account, which can be approximated with the assumption of (classical) diffusive transport,

$$L \propto T^{\beta/2} = T^{1/2} \ , \tag{13}$$

with the transport coefficient $\beta = 1$. We call this model the *standard fractal-diffusive self-organized criticality (FD-SOC)* model, defined by $[d = 3, \gamma = 1, \beta = 1]$, while the generalized FD-SOC model allows for variable coefficients $[d, \gamma, \beta]$ and alternative dimensionalities $(d = 1, 2)$.

## 4. DISCUSSION

Synthesized power law distributions have been constructed earlier, such as from nanoflares to large solar flares (Aschwanden et al. 2000), from thermal to nonthermal energies (Li et al. 2012), for magnetic energies from bright points to large active regions (Parnell et al. 2009), from solar and stellar data (Shibayama et al. 2013), from bolometric energies based on solar, stellar, lunar, and terrestrial records (Schrijver et al. 2011, 2012). What is new here is the application of the FD-SOC model into the solar-stellar flare statistics, which predicts flare energies over an unprecedented scaling range of 13 orders of magnitude.

### 4.1. *Synthesized Solar-Stellar Size Distribution*

We carry out a synthesized size distribution (Fig. 1) that can be characterized with a power law function,

$$N(E)dE = N_0[t, T] \left( \frac{E}{E_0} \right)^{-\alpha_E} dE \ , \tag{14}$$

where $E$ is the total flare energy (in units of erg), $\alpha_E$ is the power law slope, $E_0$ is an arbitrary reference value, or a threshold value, $N_0(t, T)$ is a normalization constant that depends on the start time $t$ and duration $T$ of the observations in the data sampling.

The construction of such a synthesized size distribution is shown in Fig.(1), stringed together from 5 different data sets with different flare energy ranges. A total of 15 data sets are listed in Table 1, characterized with their energy ranges $[E_{min}, E_{max}]$ and power law slopes $\alpha_E$, from which only 5 data sets are represented in the synthesized size distribution, while the other 10 cases have some inconsistencies as described in the observation Section 2.1.

What Fig.(1) shows is that each of the 5 displayed data sets exhibit a power law distribution that is consistent with the theoretical FD-SOC model with a slope of $\alpha_E = (5/3) \approx 1.67$. All 5 cases show also a turnover at the lower end of the size distributions, which is well-understood in terms of incomplete sampling below the detection threshold. The term "incomplete" refers to the scale-free probability property, which implies a reciprocality between the event frequency $N(E)$ and the SOC parameter $E$ (Eq. 8).

The graphical representation in Fig. (1) serves mostly to illustrate the invariance of power law slopes $\alpha_E$ in each data set, while the flaring frequency ($N(E)$, Eq. 14) is subject to different start times $t$, observational duration $T$, and differences in the intrinsic energy ratios $q = E_1/E_2$. For instance, energy closure of flare energies demonstrated ratios of $q = E_{elec}/E_{magn} = 0.51 \pm 0.17$ for electron energies between nonthermal electron energies and dissipated magnetic energies, $q = E_{ions}/E_{magn} = 0.17 \pm 0.17$ for ion energies, $q = E_{CME}/E_{magn} = 0.07 \pm 0.14$ for coronal mass ejection (CME) energies, and $q = E_{heat}/E_{magn} = 0.07 \pm 0.17$ for direct heating processes, which added together fulfill energy closure, $q = E_{sum}/E_{magn} = 0.87 \pm 0.18$ for the sum of all energies. This suggests that a realistic evaluation of flare energies requires the summing of partial flare energies, such as thermal energies, non-thermal energies, and bolometric radiation energies (Aschwanden et al. 2017),

$$E_{tot} = E_{nt} + E_{th} + E_{bol} \ . \tag{15}$$

For solar flares, the total radiative energy $E_{\rm bol}$ in visible wavelengths amount to about 70% of the total flare energy, characterized by a blackbody temperature of $T_{\rm bol} \approx 9000$ K (Woods et al. 2004). Unfortunately, the complete energy budget and flare partition is not known for most flare energetics studies. Once all energy parameters are measured, a complete size distribution $N(E_{tot})$ may be inferred that has the synthesized distribution as shown in Fig. (1).

### 4.2. *Flux and Fluence Limits*

The flux is defined in physical units of [energy/time], usually measured at the (background-subtracted) peak flux $F$ at the peak time $t_p$ of an event,

$$F = \max\left[f(t = t_p)\right] - f_{\rm BG} \ , \tag{16}$$

bound by the time range $t_1 \le t_p \le t_2$, where $f(t)$ is the time profile of the flux.

The fluences have the physical unit of [energy], and are measured by the time integral of the time profile $f(t)$. Thus, the fluences ($E$) are the time-integrated fluxes,

$$E = \int_{t_1}^{t_2} \left[f(t) - f_{\rm BG}\right] \, dt \approx F \times T \ , \tag{17}$$

for a time interval $(t_1, t_2)$ with well-defined start times $t_1$ and end times $t_2$). Combining the fluence approximation $E \approx F \times T$ (Eq. 17) with the flux-volume relationship $F \propto V$ (Eq. 11), and the fractal dimension relatonship $V \propto L^{D_V}$ (Eq. 6), we obtain the following scaling law for the length scale $L$ as a function of the flare energy $E$, with $D_V = 5/2$,

$$L(E) = E^{1/(2+D_V)} = E^{2/9} \approx E^{0.22} \ . \tag{18}$$

which yields the following limit for an energy range of 13 orders of magnitude,

$$\left(\frac{L_{max}}{L_{min}}\right) = \left(\frac{E_{max}}{E_{min}}\right)^{(2/9)} = \left(10^{13}\right)^{(2/9)} \approx 774 \ . \tag{19}$$

The predicted length scales for each order of magnitude from 1 to 13 is enumerated in Table 2. Using the scale of solar nanoflares as an estimation of the smallest SOC event, i.e., $L_{min} \approx 1$ Mm (Aschwanden et al. 2000; Cirtain et al. 2013), we would expect a maximum scale of $L_{max} = L_{min} \times 774$ Mm $\approx 1.04\ R_\odot$ for stellar flares. Leaving out the stellar flares we have an energy range of 9 orders of magnitude, which yields a range of $L_{max} = L_{min} \times 100$ Mm $\approx 0.14\ R_\odot$, which limits the maximum flare size to about the largest active region size, which represents a reasonable scaling, given the observed sizes of the largest sunspots and starspots. Schrijver (2011) estimates the size of the largest stellar flares to $L_{max} \approx (0.7 - 1.6) R_\odot$. Since flare size distributions allow us to extrapolate and predict the probability of the most extreme events, the magnitude limit of these events depends also on the detection of an exponential drop-off of their size distribution. For solar flares it appears that this finite-size effect occurs at $L_{max} \lesssim 200$ Mm (Aschwanden & Alexander 2001).

### 4.3. *Constraints on Physical Processes*

If a power law size distribution function extends over multiple size distributions, many authors conclude that a single physical process is responsible for the resulting size distributions in multiple data sets. The finding of power law size distributions is then attributed to a single universal physical process. For instance, finding a power law distribution of solar magnetic fields over more than five decades in flux, Parnell et al.(2009) suggest that all surface magnetic features are generated by the same physical mechanism, or that they are dominated by surface processes (such as fragmentation, coalescence, and cancellation) in a way which leads to a scale-free distribution. Because of the similarity of their size distributions, both solar and stellar flares are thought to be produced by a magnetic reconnection process (Pettersen 1989).

From our identification of physical processes in our samples we know that at least 3 different physical processes are at play, namely (i) thermal free-emission, (ii) nonthermal thick-target bremsstrahlung, and (iii) white-light bolometric emission. In addition, conductive and radiative losses are thought to contribute significantly to the dissipated flare energy budget (Shimizu et al. 1995). So, we have evidence for at least 5 physical processes, although the syntheseized size distribution function fits a sinlge power law distribution over 13 order of magnitudes. Thus, the invariant power law range is a necessary but not a sufficient condition for an universal physical process.

How can we remedy this dilemma of energy partition. Theoretically, we can measure the size distributions of energies separately for each energy partition and we can define the avalanche energy in terms of the total (summed) energy dissipated during a flare. Care needs to be exercised to avoid double counting of energies. For instance an electron that gets accelerated in a flare plasma, may also show up in the distribution of electrons that produce free-free bremsstrahlung. Nevertheless, energy closure in solar and stellar flares is feasible (Aschwanden et al. 2017).

## 5. CONCLUSIONS

In this study we arrived at the following results and conclusions:

1. We construct a synthesized power law distribution function over an energy range of $[E_{min}, E_{max}] = [10^{24}, 10^{37}]$ [erg] that is consistent with the theoretically predicted power law slope of $\alpha_E = (5/3) \approx 1.67$ of the *fractal-diffusive self-organized criticality (FD-SOC)* model (Fig. 1). The selected data sets (Table 1) encompass nanoflares, microflares, transient brightenings, large solar flares and stellar superflares. A subset of 5 selected data sets (out of 15) is consistent with the 3-D FD-SOC model, which are used in the synthesized size distribution. Most of the remaining 5 data sets use a 2-D model for the thermal flare energy that we consider to be unrealistic, given the numerous stereoscopic observations with the two STEREO spacecraft. This is a case where the *Occham's razor* philosophy (parsimony law) does not lead to a better model choice.

2. The observed 5 size distributions all exhibit a power law tail (AKAS inertial range) at the upper energy side, while the size distribution show a roll-over at the lower energy side, which is readily understood as incomplete sampling in a scale-free size distribution. This roll-over is caused by a threshold value in the detection of SOC avalanches.

3. The observed length scales $L$ agree with the theoretical prediction of the FD-SOC model, i.e., $L \propto E^{2/9} \approx E^{0.22}$. This scaling law has a weak energy dependence that produces a small range of 2 orders of magnitude for solar flares length scales $L$, i.e., 1 Mm $\le$ L $\le$ 100 Mm for solar flares, and a range of 3 order of magnitudes for stellar flares, i.e., 1 Mm $\le$ L $\le$ 774 Mm = 1.04 $R_\odot$, while the flare energy extends over 13 order of magnitudes, i.e., $10^{24}$ [erg] $\le$ E $\le$ $10^{33}$ [erg]. Thus the FD-SOC model allows us a prediction of the SOC avalanche length scale $L$ for any given flare energy $E$.

4. In the overall we conclude that the universality of power laws (and their slopes) is a consequence of SOC properties (fractality, classical diffusion, scale-freeness, volume-flux proportionality), rather than identical physical processes at different wavelengths.

Future studies may focus on the energy partition of solar flare events, so that the total energy can be estimated, since thermal, nonthermal, and white-light bolometric energies appear to represent only lower limits of SOC avalanches only.

## ACKNOWLEDGMENTS

*Acknowledgements:* This paper is dedicated to Carolus J.Schrijver (1958-2024) in memoriam, who contributed substantially to this study. We acknowledge constructive and stimulating discussions (in alphabetical order) with Arnold Benz, Sandra Chapman, Paul Charbonneau, Henrik Jeldtoft Jensen, Adam Kowalski, Sam Krucker, Alexander Milovanov, Leonty Miroshnichenko, Jens Juul Rasmussen, Carolus Schrijver, Vadim Uritsky, Loukas Vlahos, and Nick Watkins. This work was partially supported by NASA contract NNX11A099G "Self-organized criticality in solar physics" and NASA contract NNG04EA00C of the SDO/AIA instrument to LMSAL.

## REFERENCES

Aschwanden, M.J., Tarbell, T.D., Nightingale, W., Schrijver, C.J., Title A., Kankelborg, C.C., and Martens, P. 2000, *Time variability of the "quiet" Sun observed with TRACE. II. Physical parameters temperature evolution, and energetics of extreme-ultraviolet nanoflares*, ApJ 535, 1047-1065.

Aschwanden, M.J. and Alexander, D. 2001, *Flare plasma cooling from 30 MK down to 1 MK modeled from Yohkoh, GOES, and TRACE observatons during the Bastille day event (14 July 2000)*, SoPh 204: 93-121.

Aschwanden, M.J. and Parnell, C.E., 2002, *Nanoflare statistics from first principles: Fractal geometry and temperature synthesis*, ApJ 572, 1048-1071.

Aschwanden, M.J. 2004, *Physics of the solar corona. An Introduction*, Springer PRAXIS, Berlin, Heidelberg.

Aschwanden, M.J. 2014, *A macroscopic description of self-organized systems and astrophysical applications*, ApJ 782, 54.

Aschwanden, M.J. 2011, *Self-Organized Criticality in Astrophysics. The Statistics of Nonlinear Processes in the Universe*, Springer-Praxis: New York, 416p.

Aschwanden, M.J. 2015, *Thresholded power law size distributions of instabilities in astrophysics*, ApJ 814.

Aschwanden, M.J. 2013a, in *Theoretical Models of SOC Systems*, chapter 2 in *Self-Organized Criticality Systems* (ed. Aschwanden M.J.), Open Academic Press: Berlin, Warsaw, p.21.

Aschwanden,M.J. 2013b, *Self-Organized Criticality Systems in Astrophysics (Chapter 13)*, in "Self-Organized Criticality Systems" (ed. Aschwanden,M.J.), Open Academic Press: Berlin, Warsaw, p.439.

Aschwanden, M.J., Crosby, N., Dimitropoulou, M., Georgoulis, M.K., Hergarten, S., McAteer, J., Milovanov, A., Mineshige, S., Morales, L., Nishizuka, N., Pruessner, G., Sanchez, R., Sharma, S., Strugarek, A., and Uritsky, V. 2016, *25 Years of Self-Organized Criticality: Solar and Astrophysics*, Space Science Reviews 198, 47.

Aschwanden, M.J., Caspi, A., Cohen, C.M.S., Gordon, H., Jing, J., Kretzschmar, M. et al. 2017, *Coronal energetics of solar flares. V. Energy closure and coronal mass ejections*, ApJ 836/1, article id.17, 17pp.

Aschwanden, M.J. 2021, *Finite system-size effects in self-organizing criticality systems*, ApJ 909, 69.

Aschwanden, M.J. and Guedel, M. 2021, *Self-organized criticality in sellar flares*, ApJ 910, id.41, 16pp.

Aschwanden, M.J. 2022, *The fractality and size distributions of astrophysical self-organized criticality systems*, ApJ 934 33

Aschwanden, M.J. and Gogus, E. 2025, *Testing the universality of self-organized criticality in galactic, extra-galactic, and black-hole systems*, ApJ, 978:19 (11pp).

Aschwanden, M.J. 2025, *Power Laws in Astrophysics. Self-Organzed Criticality Systems*, Cambridge University Press: Cambridge.

Bak, P., Tang, C., and Wiesenfeld, K. 1987, *Self-organized criticality: An explanation of 1/f noise*, Physical Review Lett. 59(27), 381.

Bak, P. 1996, *How Nature Works. The Science of Self-Organized Criticality*, Copernicus: New York.

Benz, A.O. and Krucker, S. 2002, *Energy distribution of microevents in the quiet solar corona*, ApJ 568, 413-421.

Borucki, W.J., Koch, D., Gibor, B., Batalha, N.B., Brown, T., et al. 2010, *Kepler planet-detection mission: Introduction and first results*, Science 327, Issue 5968, 977.

Bromund, K.R., McTiernan, J.M., Kane, S.R. 1995, *Statistical studies of ISEE3/ ICE observations of impulsive hard X-ray solar flares*, ApJ 455, 733-745.

Brown, J.C. 1971, *The deduction of energy spectra of non-thermal electrons in flares from the observed dynamic spectra of hard X-ray bursts*, SoPh 18, 489.

Cai, Y., Hou, Y., Li, T., Liu, J. 2004, *Statistics of solar white-flight flares. I. Optimization and application of identification methods*, ApJ 975:69 (16pp).

Christe, S., Hannah, I.G., Krucker, S., McTiernan, J., and Lin, R.P. 2008, *RHESSI microflare statistics. I. Flare-finding and frequency distributions*, ApJ 677, 1385-1394.

Crosby, N.B., Aschwanden, M.J., and Dennis, B.R. 1993, *Frequency distributions and correlations of solar flare parameters*, SoPh 143, 275-299.

Davenport, J.R.A. 2016, *The Kepler catalog of stellar flares*, ApJ 829:23 (12pp).

Dennis, B.R. 1985, *Solar hard X-ray bursts*, Sol.Phys. 100, 465-490.

Hannah, I.G., Christe, S., Krucker, S., Hurford, G.J., Hudson, H.S. Lin P.R. 2008, *RHESSI microflare statistics. II. X-ray imaging, spectroscopy, and energy distributions*, ApJ 677:704-718.

Krucker, S. and Benz, A.O. 1998, *Energy distribution of heating processes in the quiet solar corona*, ApJ 501, L213.

Li, Y.P., Gan, W.Q., and Feng, L. 2012, *Statistical analyses on thermal aspects of solar flares*, ApJ 747, 133 (8pp).

Lu, E.T., Hamilton, R.J., McTiernan, J.M., and Bromund, K.R. 1993, *Solar flares and avalanches in driven dissipative systems*, ApJ 412, 841-852.

Mandelbrot, B.B. 1977, *Fractals: form, chance, and dimension*, Translation of *Les objects fractals*, W.H. Freeman, San Francisco.

McAteer,R.T.J., Aschwanden,M.J., Dimitropoulou,M., Georgoulis,M.K., Pruessner, G., Morales, L., Ireland, J., and Abramenko,V. 2016, *25 Years of Self-Organized Criticality: Numerical Detection Methods*, SSRv 198, 217.

Namekata, K., Sakaue, T., Watanabe, K., Asai, A., Shibata, K., et al. 2017a, *Statistical studies of solar white-light flares and comparisons with superflares on solar-type stars*, ApJ 851/2, id.91, 14pp.

Namekata, K., Sakaue, T., Watanabe, K., Asai, A., and Shibata, K. 2017b, *Validation of a scaling law for the coronal magnetic field strength and loop length of solar and stellar flares*, PASJ 69/1, id.7 10pp.

Parnell,C.E. and Jupp,P.E. 2000, *Statistical analysis of the energy distribution of nanoflares in the quiet Sun* ApJ 529, 554-569.

Parnell, C.E., DeForest, C.E., Hagenaar, H.J., Johnston, B.A., Lamb, D.A., and Welsch, B.T. 2009, *A Power-Law Distribution of Solar Magnetic Fields Over More Than Five Decades in Flux*, ApJ 698, 75-82.

Paudel, R.R., Gizis, J.E., Mullan, D.J., Schmidt, S.J., Burgasser, A.J. and Williams, P.K.G. 2020, *K2 Ultra dwarfs survey - IV. Whie light superflares observed on an L5 dwarf and flare rates of L dwarfs*, MNRAS 494, 5751-5760.

Pettersen, B.R. 1989, *A review of stellar flares and their characteristics*, SoPh 121/1-2, pp.299-312.

Pruessner, G. 2012, *Self-Organised Criticality. Theory, Models and Characterisation*, Cambridge University Press: Cambridge.

Sharma,A.S., Aschwanden,M.J., Crosby,N.B., Klimas,A.J., Milovanov,A.V., Morales,L., Sanchez,R., and Uritsky,V. 2016, *25 Years of Self-Organized Criticality: Space and Laboratory Plamsas*, SSRv 198, 167.

Schrijver, C.J. 2011, *Solar energetic events, the solar-stellar connection, and extreme space weather*, (ed., Johns-Krull, C.M., Browning, M.K., and West,A.A.; San Francisco: Astronomical Society of the Pacific), ASP Conf.Ser. 448, p.231.

Schrijver, C.J., Beer, J., Baltensperger, U., CLiver, E.W., et al. 2012, *Estimating the frequency of extremely energetic solar events, based on solar, stellar, lunar, and terrestrial records*, JGR (Space Physics) 117, 8103.

Shibayama, T., Maehara, H., Notsu, Y., Nagao, T., Satoshi,, H. et al. (2013), *Superflares on solar-type stars observed with Kepler. I. Statistical properties of superflares*, ApJSS 209/1, article id.5, 13pp.

Shimizu, T. 1995, *Energetics and occurrence rate of active region transient brightenings and implications for the heating of the active-region corona*, PASJ 47, 251-263.

Watkins, N.W., Pruessner, G., Chapman, S.C., Crosby, N.B., and Jensen, H.J. *25 Years of Self-organized Criticality: Concepts and Controversies*, 2016, SSRv 198, 3.

Woods, T.N., Eparvier, F.G., Fontenla, J., Harder, G., Kopp, W.E. et al. 2004, *Solar irradiance variability during the October 2003 solar storm period*, Geophys.Res.Let. 31, L10802.

Yang, Y. and Liu, J. 2019, *The flare catalog and the flare activity in the Kepler mission*, ApJSS 241:29 (19pp).

**Table 1.** The energy ranges $[E_{min}, E_{max}]$ and power law slopes $\alpha_E$ of solar and stellar flare energies.

| Object, Instrument | Energy range (erg) $[E_{min}, E_{max}]$ | Power law slope $\alpha_E$ | References |
|---|---|---|---|
| **Thermal energy $E_{Th}$:** | | | |
| Solar flares, SXT/Yohkoh | $[10^{25} - 10^{29}]$ | 1.5−1.6 | Shimizu (1995), Fig.11 |
| Solar flares, EIT/SOHO | $[10^{24.9} - 10^{26.3}]$ | 2.3−2.6 | Krucker & Benz (1998), Fig.2 |
| Solar EUV nanoflares TRACE | $[10^{24} - 10^{26}]$ | 1.79 | Aschwanden et al.(2000), Fig.10 |
| Solar flares, TRACE | $[10^{23} - 10^{26}]$ | 2.4−2.6 | Parnell & Jupp (2000), Figs.1,4,5 |
| Solar EUV nanoflares, EIT/SOHO | $[10^{25} - 10^{27}]$ | 2.31 | Benz & Krucker (2002), Figs.4,5,8 |
| Solar flares, GOES | $[10^{24} - 10^{32}]$ | 2.38 | Li et al. (2012), Fig.7 |
| **Non-thermal energy $E_{NT}$:** | | | |
| Solar flares, HXRBS/SMM | $[10^{25} - 10^{32}]$ | 1.53±0.02 | Crosby et al.(1993), Fig.6 |
| Solar flares, ISEE-3/ICE | $[10^{27} - 10^{33}]$ | 1.47±0.04 | Lu et al.(1993), Fig.8 |
| Solar flares, ISEE-3/ICE | $[10^{29} - 10^{30}]$ | 1.67−1.74 | Bromund et al.(1995), Table 1 |
| Solar microflares, RHESSI | $[10^{24} - 10^{30}]$ | 2.0 | Hannah et al.(2008), Fig. 18) |
| **White-light radiative energy** $E_{wl}$: | | | |
| Stellar flares KEPLER KIC | $[10^{33} - 10^{36}]$ | 1.56, 1.98 | Davenport (2016), Fig.6 |
| Stellar flares KEPLER G-type stars | $[10^{32} - 10^{37}]$ | 1.96±0.04 | Yang & Liu (2019), Fig.3 |
| Stellar flares GOES class X,M,C | $[10^{28} - 10^{32}]$ | ... | Cai et al.(2024), Fig.9 |
| Stellar flares L dwarfs | $[10^{33} - 10^{34}]$ | ... | Paudel et al.(2024), Fig.4 3 |
| Stellar flares solar-type | $[10^{29} - 10^{36}]$ | ... | Namekate et al.(2017a), Figs.6,8,12 |
| **Synthesized energy distributions:** | | | |
| EUV + SXR + HXR | $[10^{24} - 10^{32}]$ | 1.80 | Aschwanden et al.(2000), Fig.10 |
| EUV + SXR | $[10^{24} - 10^{30}]$ | 1.54±0.03 | Aschwanden & Parnell (2002), Fig.10 |
| TB + QS + AR | $[10^{24} - 10^{30}]$ | 1.54±0.05 | Aschwanden (2004), Fig. 9.27 |
| QS + AR | $[10^{17} - 10^{23}$ Mx$]$ | 1.85±0.14 | Parnell et al. (2009), Fig.5 |
| EUV + SXR + HXR + SF | $[10^{24} - 10^{35}]$ | 1.87±0.10 | Schrijver et al. (2011), Fig.3 |
| EUV + SXR + HXR + SF | $[10^{24} - 10^{37}]$ | 2.30 | Schrijver et al. (2012), Fig.3 |
| EUV + SXR + HXR | $[10^{24} - 10^{32}]$ | 2.0−2.3 | Li et al. (2012), Fig.7 |
| EUV + SXR + HXR + SF | $[10^{24} - 10^{36}]$ | 1.80 | Shibayama et al. (2013), Fig. 13.12 |

EUV=extreme ultraviiolet, SXR=soft X-rays, HXR=hard X-rays, TB=Transient brightenings, QS=Quiet Sun, AR=Active regions, SF=Stellar flares.

**Table 2.** Predicted scaling law of length scales $L(E)$ as a function of the solar and stellar flare energies $E$.

| Relative energy logarithm | Absolute energy logarithm | Relative energy factor | Predicted length scale $L(E)$ [Mm] | Nomenclature |
|---:|---:|---:|---:|---|
| 0 | 24 | 1 | 1.00 Mm | Nanoflares |
| 1 | 25 | 10 | 1.67 Mm | |
| 2 | 26 | 100 | 2.78 Mm | |
| 3 | 27 | 1,000 | 4.64 Mm | Microflares |
| 4 | 28 | 10,000 | 7.74 Mm | |
| 5 | 29 | 100,000 | 12.9 Mm | |
| 6 | 30 | 1,000,000 | 21.5 Mm | Large solar flares |
| 7 | 31 | 10,000,000 | 35.9 Mm | |
| 8 | 32 | 100,000,000 | 59.9 Mm | |
| 9 | 33 | 1,000,000,000 | 100 Mm | Stellar flares |
| 10 | 34 | 10,000,000,000 | 167 Mm | |
| 11 | 35 | 100,000,000,000 | 278 Mm | |
| 12 | 36 | 1,000,000,000,000 | 464 Mm | |
| 13 | 37 | 10,000,000,000,000 | 774 Mm | Stellar superflares |

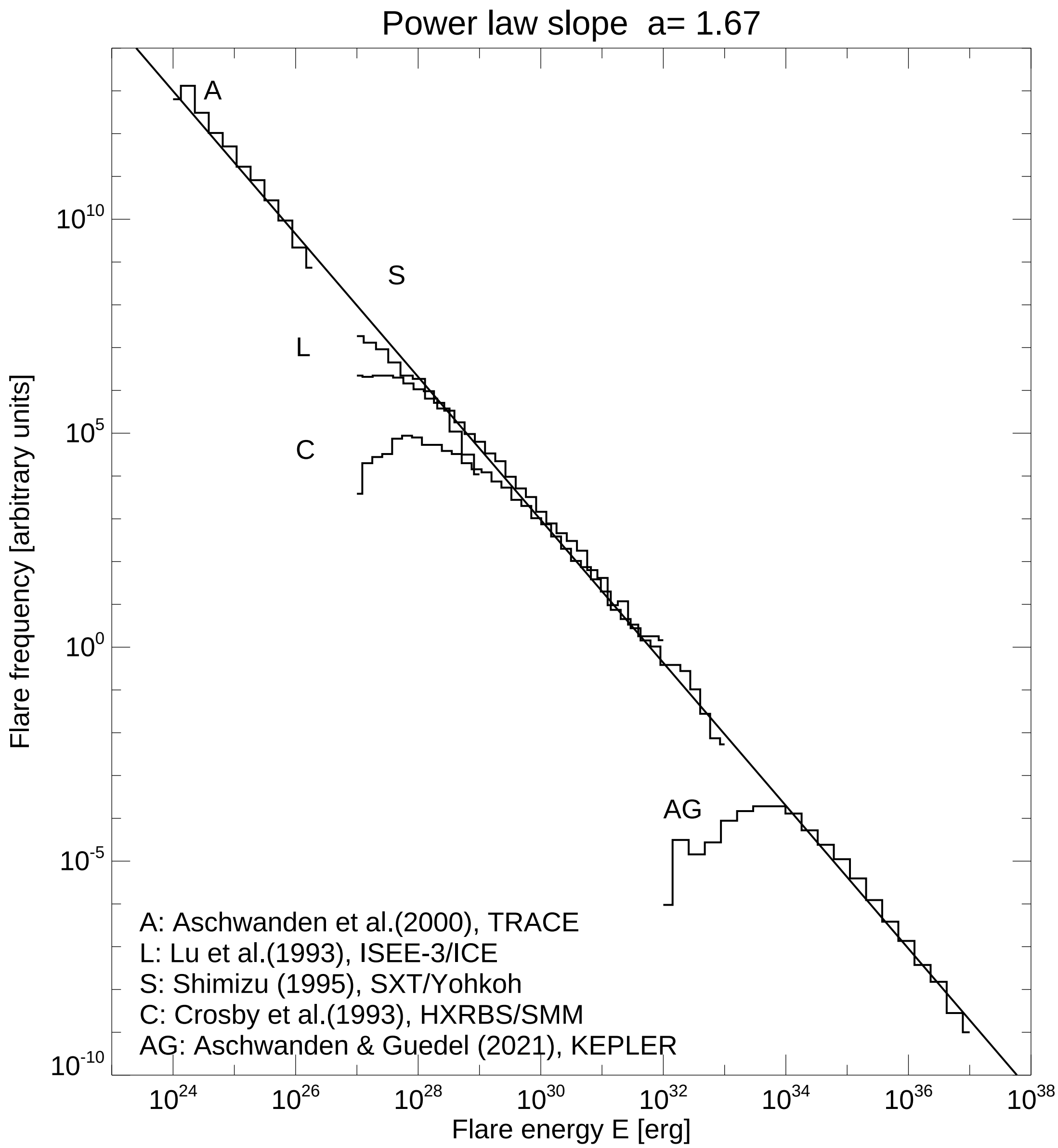


**Figure 1.** Energy size distributions synthesized from solar observations with HXRBS/SMM, ISEE-3/ICE, SXT/Yohkon, TRACE, and from stellar observations with KEPLER. The theoretical prediction of the power law slope for the flare energy distribution is $\alpha_E = 1.67$ in the FD-SOC model. The flare frequencies are aligned to the predicted power law size distribution.